Applied Catalysis A: General 447–448 (2012) 60–66

Contents lists available at SciVerse ScienceDirect

Applied Catalysis A: General

journal homepage: www.elsevier.com/locate/apcata

One-pot solvothermal synthesis of mixed Cu-Ce-O_x nanocatalysts and their catalytic activity for low temperature CO oxidation

Driss Mrabet, Ahmed Abassi, Robenson Cherizol, Trong-On Do*

Department of Chemical Engineering, Laval University, Quebec G1V 0A6, Canada

ARTICLE INFO

Article history:
Received 6 July 2012
Received in revised form 29 August 2012
Accepted 3 September 2012
Available online 11 September 2012

Keywords:
Binary Cu-Ce-O_x nanocatalyst
Nanostructure
Porous materials
Mutual interaction
CO oxidation

ABSTRACT

One-pot solvothermal method has been developed for the synthesis of high-surface area Cu-Ce-O_x binary nanocatalysts with various Cu contents in the presence of oleylamine as capping agent. The obtained binary nanocatalysts were characterized by different techniques including XRD, H_2-TPR, TEM, BET and XPS. The influence of Cu contents on their catalytic performance for the CO oxidation was also studied. Our results revealed that the Cu-Ce-O_x binary nanocatalysts show the better catalytic activity compared to those of the conventional Cu-Ce-O_x, bare nano-CeO_2 and nano-CuO catalysts. This is ascribed to mutual interaction and synergistic effect between copper oxide species and cerium oxide. Among the obtained nanocatalysts, the Cu-Ce-O_x nanocatalyst with 5.6 wt% Cu (noted as 5.6-Cu-Ce-O_x) exhibits the best catalytic activity; the 50% CO conversion can be reached at 55 °C. H_2-TPR profiles show two reduction peaks at low and high temperatures for these catalysts, which could be attributed to the reduction of highly dispersed CuO on the CeO_2 surface and the bulk-like CuO species, respectively. Using the one-pot solvothermal synthesis developed in this study, 6–8 wt% Cu content is needed for the high catalytic activity for the CO oxidation at low temperature.

1. Introduction

Precious-metal based catalysts such as Au/TiO_2, Au/CeO_2 and Pt/SnO_2 have high activity for low temperature carbon monoxide (CO) oxidation; however, due to the high cost of precious-metals, the development of efficient catalysts based on non-precious metals for catalytic oxidations is highly desired [1,2]. Among them, Cu-Ce-O_x catalysts attract special interest owing to their low cost and remarkable activities [3] that can even be compared to the precious-metals based catalysts for various reactions, such as water gas shift (WGS) [4,5], preferential CO oxidation and the oxidations of methanol and methane [6,7]. The role of ceria is not only related to its so-called oxygen storage capacity (OSC): take up oxygen under oxidizing conditions and release it under reducing ones; but also to improve dispersion of the base metals [1–7]. In addition, the presence of oxygen mobility in the CeO_2 lattice is important for the catalysts, since the oxygen is available for CO oxidation. Sedmak et al. [8,9] showed that the lattice oxygen in CeO_2 was highly involved in the catalytic reaction; because the Cu-Ce-O_x catalyst can catalyze CO oxidation even without oxygen in the reaction gas. Furthermore, Liu and Flytzani-Stephanopoulos [3,10] reported that the Cu-Ce-O_x nanocatalysts exhibited catalytic activity superior to the conventional Cu-based catalysts for CO oxidation; and these catalysts were as active as Pt based catalysts. This is due to the fact that the high surface area of nanosized ceria provides exposed active Cu sites and high oxygen vacancies resulting in better catalytic activity. In our previous work [11], we reported that the porous copper-metal oxide solids assembled from pre-synthesized metallic cupper and metal oxide nanoparticles (TiO_2 or CeO_2) in which two distinct nanoparticles (metal and metal oxide) are mutually dispersed forming porous hybrid materials [11]. These materials showed better catalytic activity for CO oxidation than those of commercial noble metal catalysts (Pt/Al_2O_3) and the conventional copper based catalysts. This also implies that nano-oxide support such as CeO_2 and TiO_2 may not simply act as a support, but also may play a direct role in the catalytic process. The homogenous distribution of copper and ceria nanoparticles in the material as well as its nanostructure have been suggested to greatly influence on the catalytic activity of CO oxidation. Furthermore, the synergetic interaction between metal and metal oxide NPs at the nano-scale interface plays a crucial role in the catalytic activity owing to facile redox interplay between copper and cerium redox couples (Cu^{2+}/Cu^{+} and Ce^{4+}/Ce^{3+}) [7,11,12].

For the type of mixed metal oxide nanomaterials, a number of preparation methods are described in the literature, including co-precipitation [3,4], precipitation–deposition [13], impregnation [14], solution combustion [15], inert gas condensation [16], reverse microemulsion [15–17], flame spray pyrolysis [6] and surfactant-templated method [17,18]. These preparations produce powders formed by nanosized crystals with BET surface areas between 20

* Corresponding author. Tel.: +1 418 656 3774; fax: +1 418 656 5993.
E-mail address: Trong-On.Do@gch.ulaval.ca (T.-O. Do).

0926-860X/$ – see front matter © 2012 Elsevier B.V. All rights reserved.
http://dx.doi.org/10.1016/j.apcata.2012.09.005

and 90 m^2/g. High catalytic activities have been demonstrated with catalysts in which copper oxide is homogeneously distributed on the ceria surface.

Among these preparations, solvothermal method is a powerful tool to synthesize metal oxide nanocrystals with controlled shape and size [11,19–23]. For most of these processes, a common feature is the use of surfactants as stabilizing agents so that formed nanocrystals are highly dispersed in solvent medium. Using these procedures, a wide variety of metal and metal oxide nanocrystals have been successfully obtained [24,25]. Although, simple metal oxide nanocrystals of CeO_2 [26,27] or CuO [28,29] have been synthesized, to our knowledge, little studies have been reported in the direct solvothermal synthesis of Cu-Ce-O_x binary system with high surface area.

In this work, we report one-pot solvothermal method for the synthesis of Cu-Ce-O_x binary system with various Cu contents (from 3 to 20 wt%) in presence of oleylamine as a stabilizing agent. We have selected copper-ceria as a catalytic system due to its attractive catalytic properties, however, this method can be extended to other catalytic binary/ternary systems such copper-alumina, copper-silver-ceria. The obtained Cu-Ce-O_x binary nanomaterials are characterized and subsequently used as nanocatalysts for the CO oxidation, compared to conventional catalysts.

2. Experimental

2.1. Sample preparation

The binary oxide Cu-Ce-O_x nanoparticles with different copper contents (from 0 to 20 wt%) were synthesized via the non-hydrolytic method using $Ce(NO_3)_3$ $6H_2O$ and $Cu(NO_3)_2$ $3H_2O$ as Ce and Cu sources, oleylamine as capping agent in toluene medium. In a typical synthesis, 0.5 g (1.15 mmol) of cerium nitrate ($Ce(NO_3)_3$, $6H_2O$) was added to 50 ml of toluene containing 5.4 g (20.2 mmol) of oleylamine and a desired amount of $Cu(NO_3)_2$ $3H_2O$. The mixture was stirred vigorously for 1 h in room temperature. The resulting clear mixture solution was sealed in a Teflon-lined stainless-steel autoclave of 80 mL capacity and heated at 180 °C for 18 h. The autoclave was then cooled down to room temperature naturally and the product of nanoparticles was precipitated with an excess ethanol and further isolated by centrifugation. The resulting solid products were dried at 100 °C and calcined at 550 °C for 4 h. For comparison, two samples, bare CeO_2 and CuO nanoparticles were also prepared, using the same procedure, except that no copper and cerium precursors were added, respectively.

2.2. Catalyst characterization

TEM examination was performed on JEOL JEM 1230 Transmission electron microscope operating at 120 kV. The nanoparticles were dispersed in toluene solution were cast onto a 200 mesh carbon-coated copper grid sample followed by evaporation at room temperature.

XRD patterns were recorded on a Siemens D5000 X-ray diffractometer using filtered Cu Kα (λ = 1.54062 Å) radiation (40 kV, 30 mA). The data were collected in a range 2θ of 20°–80° with a scan step of 0.02° and an acquisition time of 1.2 s per step. The average crystallite size was calculated using from the broadening of the XRD peaks using the Scherrer formula: $d = 0.9\lambda/(w - w_1)\cos(\theta)$; where d is the crystal diameter, w and w_1 are the half-intensity width of the relevant diffraction peak and the instrumental broadening, respectively, λ is the X-ray wavelength and θ is the angle of diffraction. The peak at 28.6° corresponding to (1 1 1) plan reflexion was used for fluorite crystal size determination.

N_2 adsorption–desorption isotherms were obtained at 77 K on Autosorb-1 apparatus. Samples were degassed under a vacuum of 10^{-5} Torr for 6 h at 200 °C prior to analysis. Surface areas were determined by the BET. X-ray Photoelecton Spectroscopy (XPS) measurements were carried out on a photoelectron spectrometer (KRATOS AXIS-ULTRA) with 225 W Al Kα radiation ($h\nu$ = 1486.6 eV) as X-ray source. The high resolution spectra were obtained with pass energy of 160 eV, with a step size of 0.1 eV, an operating pressure of 10^{-9} Torr and an acquisition time of 5.75 min. The carbonaceous C 1s line (284.6 eV) was used as the reference to calibrate the binding energy.

Temperature-programmed reduction under H_2 environment (H_2-TPR) was performed in a conventional flow apparatus with a TCD detector. Typically, 100 mg of Cu-Ce-O_x catalyst was first pretreated with 5% O_2-He at 550 °C for 1 h followed by cooling down to the room temperature. The sample was purged with 20 cm^3/min of He for 30 min to remove the physic-sorbed O_2 and then heated under a 20 cm^3/min flow rate of 5% H_2/Ar stream with temperature rising up (5 °C/min) to 600 °C, H_2 consumption was monitored continuously by TCD using a flow of 20 cm^3/min of 5% H_2/Ar as reference gas.

The copper content of the prepared samples were analyzed by atomic absorption spectroscopy (AAS) using a PerkinElmer 1100B spectroscopy after the samples were dissolved in a mixture of 25 ml of 10% HCl and 2 ml of concentrated HF at 60 °C for 24 h.

2.3. Catalytic activity

Catalytic activity tests were performed at atmospheric pressure under steady-state in a continuous-flow fixed-bed micro reactor filled with 120 mg of catalyst at different temperatures. The total flow rate of the reaction gas was 96 ml/min with the composition in vol.% of 3.5% CO and 15% O_2 balanced with helium (He). The composition of the influent and effluent gas was analyzed by an online HP 5890 gas chromatograph equipped with a carboxen-1010 PLOT column and a thermal conductivity detector (TCD) detector. The CO conversion was calculated from the change in CO concentration in the inlet and the outlet gases using the calibration curve.

3. Results and discussion

3.1. Characterization of materials

One-pot synthesis of a series of binary oxide Cu-Ce-O_x nanocrystals with different copper contents was performed in organic solvent medium in the presence of oleylamine a capping agent. Table 1 summarizes the physico-chemical properties of this series of calcined catalysts and designated as [x]-Cu-Ce-O_x, where x is Cu/Cu + Ce content in wt%. For comparison, two samples: bare CeO_2 and CuO nanoparticles were also prepared using the same procedure, except that no copper and cerium precursors were added, respectively. The mean size of bare CeO_2 and CuO is 7 nm and 5 nm, respectively (not shown). Furthermore, the sample of 10-Cu-Ce-O_x-imp which was prepared by impregnation with commercial CeO_2, was used as a reference. Since the nanocrystals are protected by alkyl chains after synthesis, the capping alkyl chains are acting as protecting agent between nanoparticles to inhibit them from aggregation during the thermal treatment. As a result, the catalysts with high surface area and high inter-particle porosity can be obtained after calcination. The alkyl chain surfactants covering the NPs can act as sacrificial spacers between the NPs, which are removed during the thermal procedure, giving rise to a porous structure. As seen in Table 1, the BET surface areas are 90 m^2/g for 2.9-Cu-Ce-O_x (at low Cu loading) and 110 m^2/g for 19.4-Cu-Ce-O_x (at high Cu loading). Interestingly, the theoretical specific surface

Table 1
Physicochemical properties of the Cu-Ce-O_x catalysts with different Cu contents after calcinations in air at 550 °C for 4 h.

Sample	Cu (wt%)	S_{BET} (m^2/g)	Crystallite size of CeO_2 (nm)		S_{th} (m^2/g)[a]
			(I)	(II)	
2.9-Cu-Ce-O_x	2.9	90	6.8	7.0	115
5.6-Cu-Ce-O_x	5.6	96	6.9	7.5	114
8.6-Cu-Ce-O_x	8.6	106	7.2	7.0	109[b]
10.6-Cu-Ce-O_x	10.6	113	6.9	7.5	114[b]
19.4-Cu-Ce-O_x	19.4	111	7.0	7.0	117[b]

The sample designated as x-Cu-Ce-O_x, where x is the percentage of copper content in weigh (Cu/Ce + Cu %).
(I) Mean crystallite size of CeO_2 determined from the XRD patterns by Scherrer equation using the XRD peak (1 1 1) at $2\theta = 28.7$ and (II) from TEM analyze over 300 nanoparticles.
[a] Surface area calculated from crystallite mean size (assuming cubic particles): $S_{th} = 6000/(\rho d)$ where ρ and d are the material density ($\rho_{ceria} = 7.65$ g/cm^3) and particle dimension (nm), respectively.
[b] The surface area is roughly calculated assuming the crystallite size of CuO the same as of CeO_2.

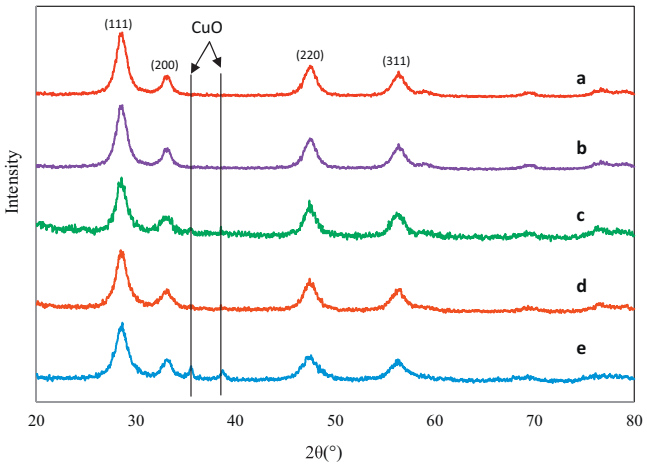

Fig. 1. XRD patterns of the Cu-Ce-O_x samples after calcinations at 550 °C for 4 h: (a) 2.9-Cu-Ce-O_x; (b) 5.6-Cu-Ce-O_x; (c) 8.6-Cu-Ce-O_x; (d) 10.6-Cu-Ce-O_x; (e) 19.4-Cu-Ce-O_x.

areas calculated from the TEM mean particle sizes, assuming cubic nanoparticles, are comparable to those obtained by the BET technique (Table 1). This indicates that the nano-particle surface was preserved after removal of protecting alkyl chains agent. Furthermore, the specific surface area slightly increases with Cu content in the range of 90–110 m^2/g. A slight increase in high surface area with increasing Cu loading could be due to the formation of small separate bulk-like CuO particles (see TEM images, Fig. 2) and the protecting agent between nanoparticles [11].

Fig. 1 shows XRD patterns of this series of calcined Cu-Ce-O_x samples. In all cases, the XRD pattern of the samples exhibits diffraction peaks characteristic of CeO_2 phase in the cubic crystal structure of fluorite-type. At low Cu content, for the samples of 2.9 and 5.6 wt% Cu (Fig. 1a and b), no XRD peaks attributed to CuO phase were detected. The absence of diffraction peaks for CuO suggests that the high dispersion and small size of Cu on the samples. The particle size of Cu is below the detection limit of the instrument under the experimental conditions (<4 nm). Indeed, formation of a solid solution of Cu-Ce-O_x was proposed by Xiaoyuan et al. [30] and Bera et al. [31]. Based on Rietvel analysis of XRD spectra, they showed a reduction in the cell parameter of ceria, due to the

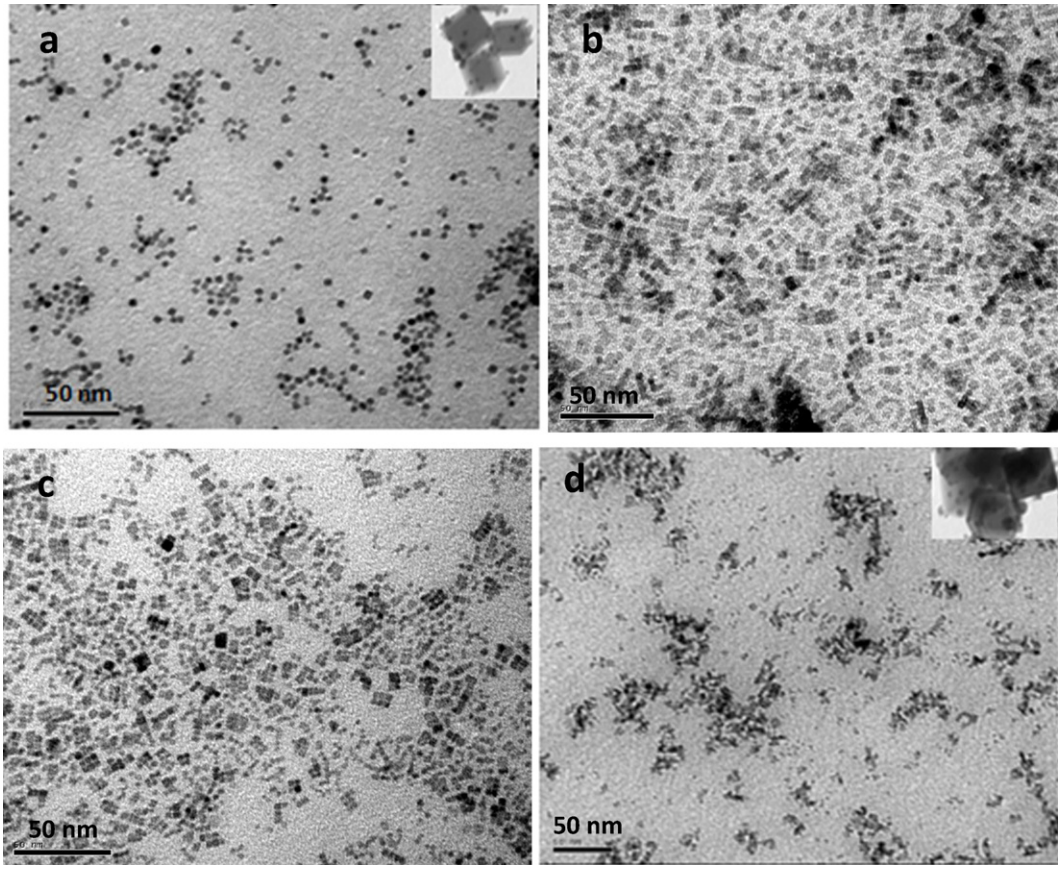

Fig. 2. TEM images of as made OL-capped Cu-Ce-O_x nanoparticles of: (a) 5.6-Cu-Ce-O_x; (b) 8.6-Cu-Ce-O_x; (c) 10.6-Cu-Ce-O_x; (d) 19.4-Cu-Ce-O_x.

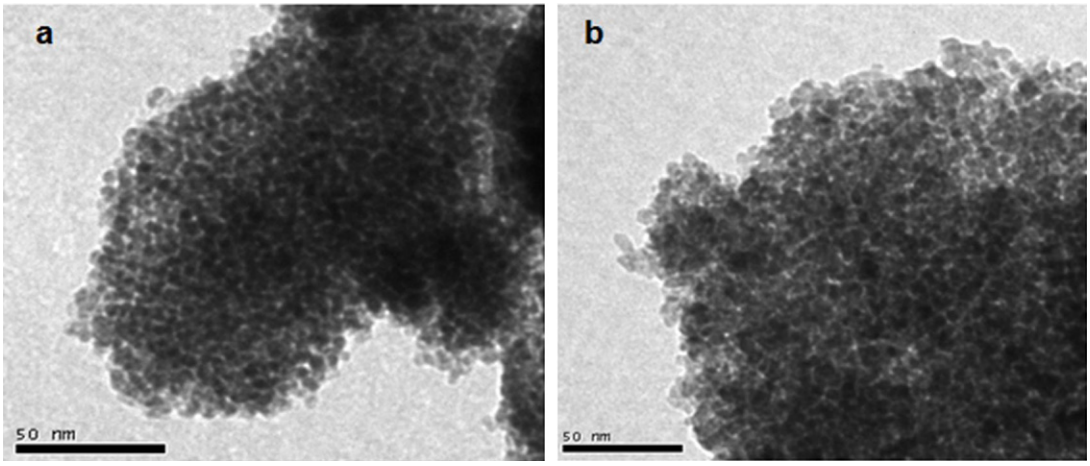

Fig. 3. TEM images of the calcined Cu-Ce-O_x nanocatalysts of: (a) 5.6-Cu-Ce-O_x, (b) 19.4-Cu-Ce-O_x.

presence of copper in the CeO_2 lattice. Furthermore it was found that when copper loading is higher than the limit of Cu^{2+} incorporated into the CeO_2 lattice, its remainder could reside on the CeO_2 surface. This also indicates in our case that at low Cu content (Cu < 8.6 wt%), very small copper oxide clusters were formed and could be partly incorporated of copper in the ceria lattice [32]. However, at higher Cu content, as seen in Fig. 1c–e, very weak reflections at 36° and 39° attributed to CuO were detected. Even at 19.4 wt% Cu, together with the CeO_2 peaks, only small broad peaks of CuO were observed.

As seen in Fig. 2a and d – inset, small copper nanoparticles and high dispersion of copper oxide on Cu-Ce-O_x nanocomposites can be attained using our solvothermal method. As reported in the several papers [33–35], CuO is in form of highly dispersed clusters on ceria, due to the similarity of the cerium and copper ionic radii. From the XRD patterns of the calcined samples in Fig. 1, the mean sizes of ceria crystallites were also calculated by the Scherrer's equation of the peak at $2\theta = 28.7°$, and the values are reported in Table 1. It can be seen that all the samples have ceria crystallites quite small in the range of 6.8–7.2 nm. Interestingly, even high Cu content (up to 19.4 wt% Cu) the average crystallite size of ceria did not change significantly.

Further, particle sizes of the samples were also observed by transmission electronic microscopy (TEM). The as-synthesized nanoparticles exhibit a rather uniform and nearly cubic shape with an average diameter of 7.0 nm for the Cu-Ce-O_x samples with low Cu content (Fig. 2a and b). However, at high Cu content (Fig. 2c and d), the nano-particles tend to aggregate. Beside of individual cubic particles, some aggregations from nanocubes were formed. It is also noted that for the 19.4-Cu-Ce-O_x sample (with high 19.4 wt% Cu content), additional small separate spherical particles were also observed (Fig. 2c and d). This could be due to separate bulk-like CuO particles with in agreement with the XRD results. The particle sizes of CeO_2 nanoparticles determined using the Scherrer's equation correspond reasonably well to those estimated from the TEM images. TEM images of the calcined 10.6-Cu-Ce-O_x and 19.4-Cu-Ce-O_x samples exhibit wormhole-type nanostructure throughout large domains (Fig. 3). The high interparticle porosity was formed; the nanoparticles retained however their individual size and shape.

XPS analysis was also carried out in order to investigate the surface nature of the prepared samples. We focused on the sample of calcined Cu-Ce-O_x with 5.6 wt% Cu (denoted 5.6-Cu-Ce-O_x), before and after different treatments: (i) the starting calcined sample and then exposed in air, (ii) the sample treated in 5 mol% O_2 balanced with helium at 150 °C for 4 h, (iii) the sample reduced in 5 mol% CO balanced with helium at 300 °C for 4 h. The O 1s XPS spectra for these samples are shown in Fig. 4. All the spectra show a peak at 529.3 eV, which is assigned to oxygen ions in CeO_2 and CuO. An evident shoulder at higher binding energies at ~533 eV is present and attributable to hydroxyl groups and/or lattice oxygen vacancies. This peak is due to highly polarized oxide ions at the surface (and interfaces) of the nano-crystals with a low coordination [32]. As seen in Fig. 4, no significant changes in intensity of the peak at 529.3 eV after the CO treatment, e.g., almost all copper reduced to Cu^+ and metallic state after this treatment (see below), as compared to that of the sample before treatment. This is due to only very small fraction of oxygen from CuO compared to that from CeO_2. Furthermore, a relatively high intensity of the peak at ~533 eV, and no significant change in its intensity after three different treatments suggests high hydroxyl groups and/or lattice

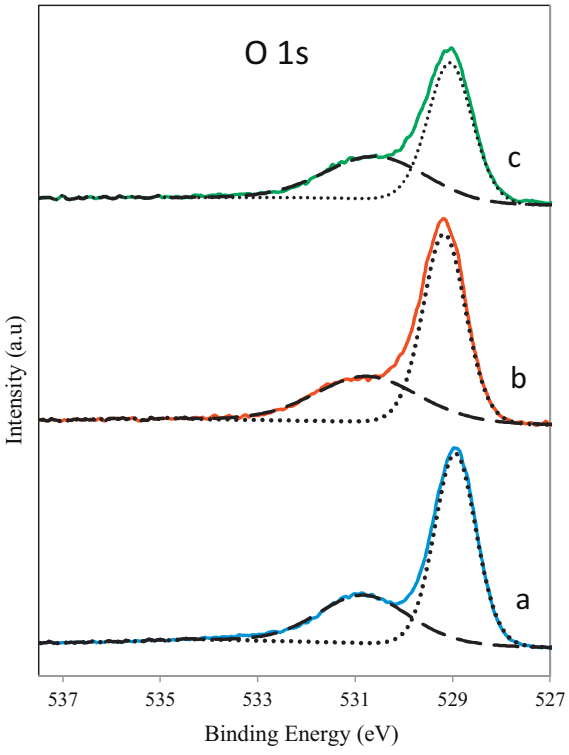

Fig. 4. O 1s high resolution XPS spectra of (a) the calcined 5.6-Cu-Ce-O_x sample at 550 °C then exposed in air; (b) after treatment in 5 mol% O_2 balance He at 150 °C; (c) after reduction in 5 mol% CO balance He at 300 °C for 4 h.

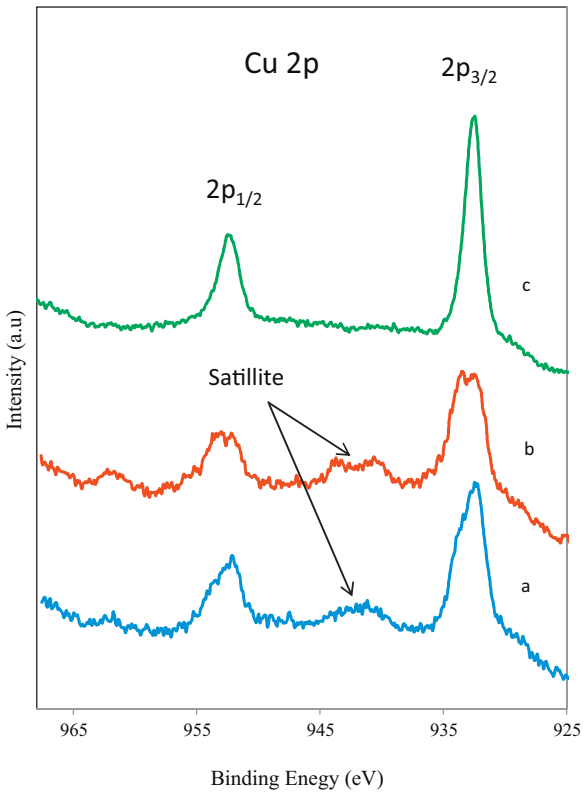

Fig. 5. Cu 2p high resolution XPS spectra of (a) the calcined 5.6-Cu-Ce-O_x sample at 550 °C then exposed in air; (b) after treatment in 5 mol% O_2 balance He at 150 °C; (c) after reduction in 5 mol% CO balance He at 300 °C for 4 h.

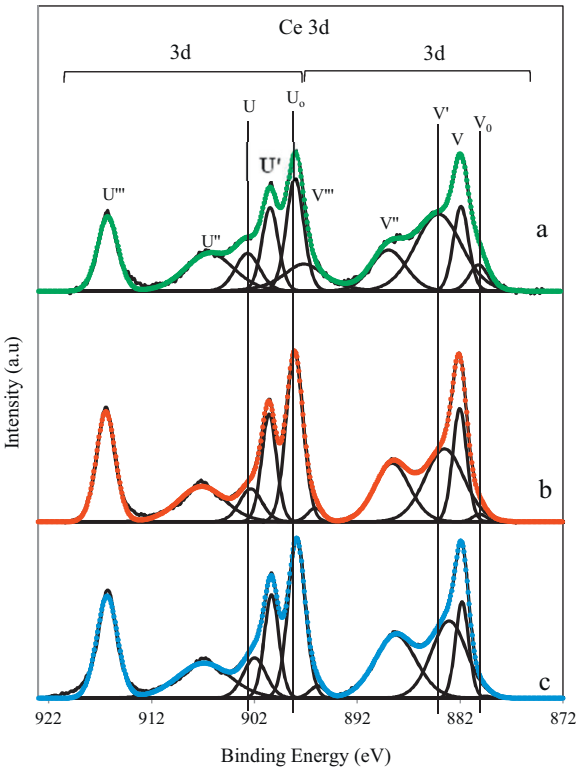

Fig. 6. Ce 3d high resolution XPS spectra of 5.6-Cu-Ce-O_x of (a) the calcined 5.6-Cu-Ce-O_x sample at 550 °C then exposed in air; (b) after treatment in 5 mol% O_2 balance He at 150 °C; (c) after reduction in 5 mol% CO balance He at 300 °C for 4 h.

oxygen vacancies in the nanocatalyst [32,36]. Fig. 5 shows Cu2p XPS spectra of these samples. For the starting sample and the samples treated in situ in O_2 at 150 °C (spectra a, b), two peaks at 932.7 eV and 952.2 eV are assigned to Cu $2p_{3/2}$ and $2p_{1/2}$ transitions, respectively. It is noted that both peaks (Cu $2p_{3/2}$ and $2p_{1/2}$) are quite broad, exhibiting a shoulder at higher binding energies (933.7 and 953.7 eV) which is typical of copper in the Cu^{2+} state. This is also confirmed by shake-up satellites (at 943.5 and 962.0 eV) typical of Cu^{2+} species. Two main peaks of Cu $2p_{3/2}$ and $2p_{1/2}$ at slightly lower binding energy also suggest the presence of Cu^{+} or metallic Cu^0 in these samples. These results are in good agreement with literature results which reported the presence of both Cu^{2+} and Cu^{+} species (or metallic Cu^0) in Cu-Ce-O_x systems [37,38]. However, for the Cu-Ce-O_x sample after reduction in CO at 300 °C, the peaks assigned to Cu $2p_{3/2}$ and $2p_{1/2}$ transitions are shifted to lower binding energy, and are intense and shape. Furthermore, no essentially shake-up satellite (at 943.5 and 962.0 eV) characteristics of Cu^{2+} species were observed. This suggests almost all copper reduced to Cu^{+} and metallic Cu^0 state after this treatment.

The XP spectra of Ce 3d core electron levels for these samples are shown in Fig. 6. The main features are composed of six peaks corresponding to the three pairs of spin–orbit doublets. These peaks, labeled V (882.4 eV), V′ (888.4 eV), U° (898.1 eV) and U′ (900.6 eV), U″ (906.9 eV), U‴ (916.4 eV) according to the convention established by Burroughs et al. [39], refer respectively to $3d_{3/2}$ and $3d_{5/2}$ of Ce(IV), suggesting that on these samples cerium is present as fully oxidized CeO_2. It must be however noted that shoulders at about 885 eV (V″) and 903 eV (U), referring to $3d_{3/2}$ and $3d_{5/2}$ respectively attributed to Ce(III), can be observed on the starting sample and the sample after treatment in oxygen at 150 °C for 4 h. However, these peaks are more evident and intense for the sample after reducing in CO balanced with helium at 300 °C suggesting a higher amount of Ce^{3+} species on this sample after this treatment.

Fig. 7 shows temperature-programmed reduction under H_2 (H_2-TPR) profiles of the Cu-Ce-O_x samples with different Cu contents after calcinations at 550 °C. For the Cu-Ce-O_x sample with low Cu content, 2.9 wt% (noted 2.9-Cu-Ce-O_x), three not well resolved reduction peaks can be observed in the range of 170–230 °C. The middle peak is more intense than the other ones. As it is well known that the reduction profiles of bulk CuO and bare CeO_2 are characterized by a single peak at ~300 °C and ~520 °C, respectively [37,40]. Furthermore, TPR profiles of the Cu-Ce-O_x samples did not show the high temperature reduction peak at about 520 °C as it is observed on bare ceria. This suggests that a mutual interaction

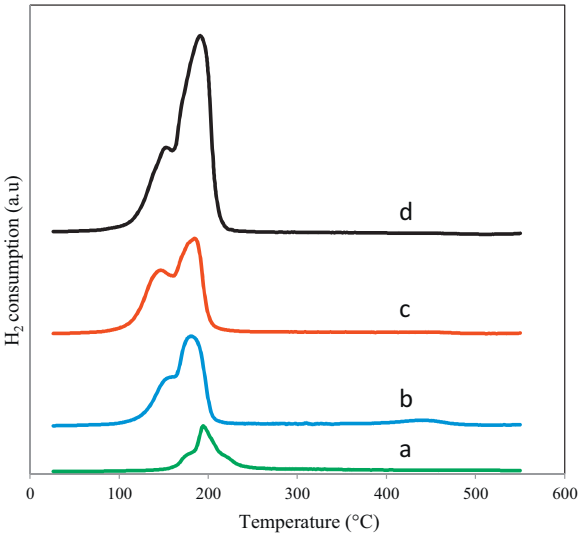

Fig. 7. H_2-TPR profiles of the calcined Cu-Ce-O_x samples with different Cu contents: (a) 2.9-Cu-Ce-O_x; (b) 5.6-Cu-Ce-O_x; (c) 10.6-Cu-Ce-O_x; (d) 19.4-Cu-Ce-O_x.

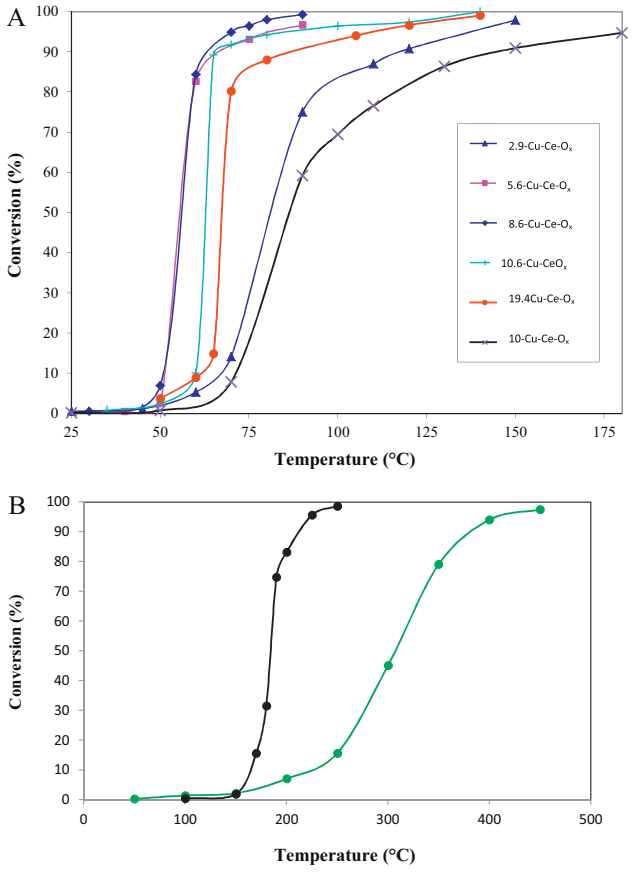

Fig. 8. CO conversion as function of reaction temperature for: (a) Cu-Ce-O_x catalysts with different Cu contents and 10% Cu-Ce-O_x prepared by impregnation, and (b) bare CeO_2 and CuO.

between ceria and copper oxide takes place, leading to an easier reduction of both ceria and CuO. Furthermore, no reduction peak for CeO_2 was observed; it could be due to its overlapping with the two reduction peaks of copper oxide [33,34,37,38].

The H_2-TPR peak temperature of the Cu-Ce-O_x sample is much lower than those of both bare ceria and CuO. This is due to the strong interaction of CuO species dispersed on the CeO_2 surface: the higher the interaction leads to the lower the reduction temperature [41]. For the samples with high Cu contents (5.6, 10.6 and 19.4 wt%), only two reduction peaks were observed. These peaks are more intense and shifted to lower temperatures. Two reduction peaks in the case of copper-ceria catalysts are probably due to different interaction degree of CuO species with ceria. The reduction peak at low temperature is attributed to CuO clusters attached on the nanoceria surface and strongly interacting with the ceria surface; the other one at higher temperature due to bulk-like as low interacting CuO species [37,38,41,42]. As seen in Fig. 6, the intensity of the reduction peak at high temperature increases with increasing Cu content. Similar results were also reported by different research groups [42–45]. They also attributed the low-temperature reduction peak to the reduction of highly dispersed CuO on the surface of CeO_2 and the higher temperature peak to "bulk-like" CuO particles.

3.2. Catalytic activity

Fig. 8 shows catalytic activity results, in terms of the conversion of CO oxidation as a function of temperature over the series of Cu-Ce-O_x nanocatalysts with different Cu contents and a catalyst of 10 wt% Cu prepared by impregnation with commercial ceria was used as a reference sample (Fig. 8a). For comparison,

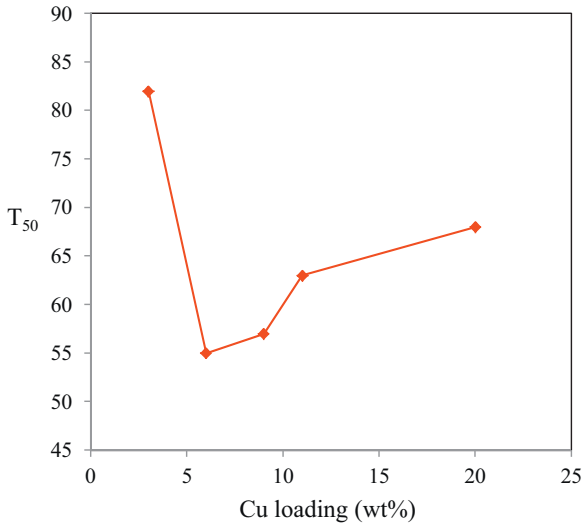

Fig. 9. Reaction temperature corresponding to the 50% CO conversion (T50) as a function of CuO content for a series of Cu-Ce-O_x nanocatalysts.

two samples of bare CeO_2 and CuO nanoparticles were prepared. Their results for the CO oxidation are reported in Fig. 8b. At each reaction temperature, the reaction was continued for about 1 h to achieve steady-state activity. It can be observed that, for the all samples, the conversion of CO increases with increasing the reaction temperature. The catalysts prepared by our one-pot synthetic method exhibit much higher catalytic activity compared to the reference sample prepared by impregnation and the samples of bare CeO_2 and CuO nanoparticles. Among all these samples, the 5.6-Cu-Ce-O_x sample exhibits the highest activity with a complete CO conversion at 80 °C. The temperature of 50% CO conversion for different samples as a function of Cu content is shown in Fig. 9. The catalytic activity of CO oxidation in terms of temperature at which the 50% CO conversion was reached is in the order: 5.6-Cu-Ce-O_x > 8.6-Cu-Ce-O_x > 10.6-Cu-Ce-O_x > 19.6-Cu-Ce-O_x > 2.9-Cu-Ce-O_x > 10-Cu-Ce-O_x impr. > CuO > CeO_2. The observed trends in the catalytic activity with variation of Cu contents correlated with the TPR results suggest that only an amount of copper at about 5–6 wt% is needed to form active sites for the CO oxidation reaction, and that an excess copper (>6 wt%) could form bulk CuO particles contributing little to the activity. The high activity of Cu-Ce-O_x (~6 wt% Cu) is related with the low reduction temperature peak of finely dispersed CuO species on catalysts (Fig. 7). The easier the reduction of the finely dispersed CuO species is the higher the oxidation activity of catalyst. The findings of this work are in agreement with the proposition that the high activity of Cu-Ce-O_x catalysts is due to the presence of highly dispersed CuO clusters in strong interaction with CeO_2, which can be easily reduced at low temperatures [3,46,47]. Active centers are created at the interface between CuO and CeO_2, as well as with highly interfacial contact [47].

This also indicates that easier reduction of CuO species on catalyst is a possible active site of CO oxidation, which can adsorb CO. On the basis of the above results, we attributed the enhanced catalytic activity due to the synergistic and strong interaction of CuO and CeO_2 nanoparticles which results in the easier reduced CuO species and CO adsorption on Cu-Ce-O_x catalyst.

4. Conclusion

A series of high-surface area nanosized Cu-Ce-O_x catalysts with different Cu contents has been prepared par one-pot solvothermal method and tested for low-temperature CO oxidation. Small

particle size (~7 nm) and high surface area (90–115 m^2/g) of the nanocatalysts can be achieved. These nanoporous catalysts are very active for the CO oxidation and show higher catalytic activity than those of 10-Cu-Ce-O_x prepared by impregnation using CeO_2 commercial and the bare CeO_2 and CuO nanocatalysts. Two reduction peaks in H_2-TPR could be due the presence of two different CuO species. The low-temperature TPR peak of Cu-Ce-O_x is attributed to the finely CuO species dispersed on the nanoceria surface, and the high-temperature one is attributed to the bulk-like CuO species. As a result, the high dispersion and mutual interaction of CuO and CeO_2 particles are responsible for low-temperature CO oxidation. This is also concluded that using the one-pot solvothermal synthesis developed in this study, 5–7 wt% Cu content is needed for the high catalytic activity for the CO oxidation.

Acknowledgments

This work was supported by the Natural Sciences and Engineering Research Council of Canada (NSERC). D.M. thanks the FQRNT for the PhD Scholarship.

References

[1] H.J. Freund, G. Meijer, M. Scheffler, R. Schlögl, M. Wolf, Angew. Chem. Int. Ed. 50 (2011) 10064–10094.
[2] R. Prasad, P. Singh, Catal. Rev.: Sci. Eng. 54 (2012) 224–279.
[3] W. Liu, M. Flytzani-Stephanopoulos, J. Catal. 153 (1995) 304–316.
[4] M. Flytzani-Stephanopoulos, X. Qi, Ind. Eng. Chem. 43 (2004) 3055–3062.
[5] J.A. Rodriguez, J. Graciani, J. Evans, J.B. Park, D. Stacchiola, S.D. Senanayake, S. Ma, M. Pérez, P. Liu, F.J. Sanz, J. Hrbek, Angew. Chem. Int. Ed. 48 (2009) 8047–8050.
[6] R. Kydd, W.Y. Teoh, K. Wong, Y. Wang, J. Scott, Q.-H. Zeng, A.-B. Yu, J. Zou, R. Amal, Adv. Funct. Mater. 19 (2009) 369–377.
[7] A. Hornés, B. Hungría, P. Bera, L. Cámara, M. Fernández-García, A. Martínez-Arias, L. Barrio, M. Estrella, G. Zhou, J.J. Fonseca, J.C. Hanson, J.A. Rodriguez, J. Am. Chem. Soc. 132 (2010) 34–35.
[8] G. Sedmak, S. Hoeevar, J. Levec, J. Catal. 222 (2004) 87–99.
[9] G. Sedmak, S. Hoeevar, J. Levec, J. Catal. 213 (2003) 135–150.
[10] W. Liu, M. Flytzani-Stephanopoulos, J. Catal. 153 (1995) 317–332.
[11] D. Mrabet, M.H. Zahedi-Niaki, T.O. Do, J. Phys. Chem. C 112 (2008) 7124–7129.
[12] S. Carrettin, P. Concepcion, A. Corma, J.M.L. Nieto, V.F. Puntes, Angew. Chem. Int. Ed. 43 (2004) 2538–2540.
[13] A. Gurbani, J.L. Ayastuy, M.P. González-Marcos, J.E. Herrero, J.M. Guil, M.A. Gutiérrez-Ortiz, Int. J. Hydrogen Energy 34 (2009) 547–665.
[14] X. Tang, B. Zhang, Y. Li, Y. Xu, Q. Xin, W. Shen, Catal. Today 93-95 (2004) 191–198.
[15] W. Shan, W. Shen, C. Li, Chem. Mater. 15 (2003) 4761–4767.
[16] A. Hornés, P. Bera, L.A. Cámara, D. Gamarra, G. Manuera, A. Martínez-Arias, J. Catal. 268 (2009) 367–375.
[17] J. Li, P. Zhu, S. Zuo, Q. Huang, R. Zhou, Appl. Catal. A: Gen. 381 (2010) 226–261.
[18] P. Zhu, J. Li, S. Zuo, R. Zhou, Appl. Surf. Sci. 255 (2008) 2903–2909.
[19] C.B.D. Murray, J.M. Norris, G. Bawendi, J. Am. Chem. Soc. 115 (1993) 8706–8715.
[20] Y.-W. Jun, J.-S. Choi, J. Cheon, Angew. Chem. Int. Ed. 45 (2006) 3414–3439.
[21] T.D. Nguyen, T.O. Do, Langmuir 25 (2009) 5322–5332.
[22] C.T. Dinh, T.D. Nguyen, F. Kleitz, T.O. Do, ACS Nano 11 (2009) 3737–3742.
[23] T.D. Nguyen, C.T. Dinh, T.O. Do, ACS Nano 4 (2010) 2263–2273.
[24] J. Park, J. Joo, S. Gu Kwon, Y. Jang, T. Hyeon, Angew. Chem. Int. Ed. 46 (2007) 4630–4660.
[25] M. Niederberger, G. Garnweitner, Chem. Eur. J. 12 (2006) 7282–7302.
[26] S. Yang, L. Gao, J. Am. Chem. Soc. 128 (2006) 9330–9331.
[27] T. Yu, J. Joo, Y. Park, T. Hyeon, Angew. Chem. Int. Ed. 44 (2005) 7411–7414.
[28] N.R. Jana, X. Peng, J. Am. Chem. Soc. 125 (2003) 14280–14281.
[29] M. Yin, C.-K. Wu, Y. Lou, C. Burda, J.T. Koberstein, Y. Zhu, S. O'Brien, J. Am. Chem. Soc. 127 (2005) 9506–9511.
[30] J. Xiaoyuan, L. Guanglie, Z. Renxian, M. Jianxin, C. Yu, Z. Xiaoming, Appl. Surf. Sci. 173 (2001) 208–220.
[31] P. Bera, K.R. Priolkar, P.R. Sarode, M.S. Hegde, S. Emura, R. Kumashiro, N.P. Lalla, Chem. Mater. 14 (2002) 3591–3601.
[32] J.P. Holgado, G. Munuera, J.P. Espinós, A.R. González-Elipe, Appl. Surf. Sci. 158 (2000) 164–171.
[33] S. Hočevar, U.O.K. Boris Orel, A.S. Aricó, H. Kim, Appl. Catal. B: Environ. 28 (2000) 113–125.
[34] Y. Li, Q. Fu, M. Flytzani-Stephanopoulos, Appl. Catal. B: Environ. 27 (2000) 179–191.
[35] L. Kundakovic, M. Flytzani-Stephanopoulos, Appl. Catal. A: Gen. 171 (1998) 13–29.
[36] A.Q. Wang, P. Punchaipetch, R.M. Wallace, T.D. Golden, J. Vac. Sci. Technol. 21 (2003) 1169–1175.
[37] G. Avgouropoulos, T. Ioannides, Appl. Catal. A: Gen. 244 (2003) 155–167.
[38] T. Tabakova, F. Boccuzzi, M. Manzoli, J.W. Sobczak, V. Idakiev, A. Andreeva, Appl. Catal. A: Gen. 298 (2006) 127–143.
[39] P. Burroughs, A. Hamnett, A.F. Orchard, G. Thornton, J. Chem. Soc. Dalton Trans. 17 (1976) 1686–1693.
[40] G. Fierro, M.L. Jacono, M. Inversi, P. Porta, R. Lavecchia, F. Cioci, J. Catal. 148 (1994) 709–721.
[41] S. Scirè, P.M. Riccobene, C. Crisafulli, Appl. Catal. B: Environ. 101 (2010) 109–117.
[42] M.F. Luo, Y.P. Song, G.Q. Xie, Z.Y. Pu, P. Fang, Y.L. Xie, Catal. Commun. 8 (2007) 834–838.
[43] C.R. Jung, J. Han, S.W. Nam, T.H. Lim, S.A. Hong, H.I. Lee, Catal. Today 93 (2004) 183–190.
[44] G. Avgouropoulos, T. Ioannides, H. Matralis, Appl. Catal. B: Environ. 56 (2005) 87–93.
[45] X.C. Zheng, X.L. Zhang, X.Y. Wang, S.R. Wang, S.H. Wu, Appl. Catal. A: Gen. 295 (2005) 142–149.
[46] M.F. Luo, Y.J. Zhong, X.X. Yuan, X.M. Zheng, Appl. Catal. A: Gen. 162 (1997) 121–131.
[47] J.B. Wang, D.H. Tsai, T.J. Huang, J. Catal. 208 (2002) 370–380.